Field penetrations in photonic crystal Fano reflectors

Deyin Zhao,[1] Zhenqiang Ma,[2] and Weidong Zhou[1,*]

[1]*Department of Electrical Engineering, NanoFAB Center, University of Texas at Arlington, Texas 76019, USA*
[2]*Department of Electrical and Computer Engineering, University of Wisconsin-Madison, Wisconsin 53706, USA*
**wzhou@uta.edu*

Abstract: We report here the field and modal characteristics in photonic crystal (PC) Fano reflectors. Due to the tight field confinement and the compact reflector size, the cavity modes are highly localized and confined inside the single layer Fano reflectors, with the energy penetration depth of only 100nm for a 340 nm thick Fano reflector with a design wavelength of 1550 nm. On the other hand, the phase penetration depths, associated with the phase discontinuity and dispersion properties of the reflectors, vary from 2000 nm to 4000 nm, over the spectral range of 1500 nm to 1580 nm. This unique feature offers us another design freedom of the dispersion engineering for the cavity resonant mode tuning. Additionally, the field distributions are also investigated and compared for the Fabry-Perot cavities formed with PC Fano reflectors, as well conventional DBR reflectors and 1D sub-wavelength grating reflectors. All these characteristics associated with the PC Fano reflectors enable a new type of resonant cavity design for a large range of photonic applications.

OCIS codes: (140.3948) Fabry-Perot cavity; (999.999) Fano resonance; (230.0230) Optical devices; (050.5080) Phase shift; (999.999) Photonic crystal.

References and links

1. S. Boutami, B. Benbakir, X. Letartre, J. L. Leclercq, P. Regreny, and P. Viktorovitch, "Ultimate vertical Fabry-Perot cavity based on single-layer photonic crystal mirrors," Opt. Express **15**(19), 12443–12449 (2007).
2. M. Sagawa, S. Goto, K. Hosomi, T. Sugawara, T. Katsuyama, and Y. Arakawa, "40-Gbit/s Operation of Ultracompact Photodetector-Integrated Dispersion Compensator Based on One-Dimensional Photonic Crystals," Jpn. J. Appl. Phys. **47**(8), 6672–6674 (2008).
3. A. Chutinan, N. P. Kherani, and S. Zukotynski, "High-efficiency photonic crystal solar cell architecture," Opt. Express **17**(11), 8871–8878 (2009).
4. O. Kilic, M. Digonnet, G. Kino, and O. Solgaard, "External fibre Fabry-Perot acoustic sensor based on a photonic-crystal mirror," Meas. Sci. Technol. **18**(10), 3049–3054 (2007).
5. J. D. Joannopoulos, S. G. Johnson, J. N. Winn, and R. D. Meade, *Photonic Crystals: Molding the Flow of Light*, 2nd ed. (Princeton University Press, 2008).
6. U. Fano, "Effects of Configuration Interaction on Intensities and Phase Shifts," Phys. Rev. **124**(6), 1866–1878 (1961).
7. R. Magnusson, and S. S. Wang, "New principle for optical filters," Appl. Phys. Lett. **61**(9), 1022 (1992).
8. S. Fan, and J. D. Joannopoulos, "Analysis of guided resonances in photonic crystal slabs," Phys. Rev. B **65**(23), 235112 (2002).
9. D. K. Jacob, S. C. Dunn, and M. G. Moharam, "Flat-top narrow-band spectral response obtained from cascaded resonant grating reflection filters," Appl. Opt. **41**(7), 1241–1245 (2002).
10. S. T. Thurman, and G. M. Morris, "Controlling the spectral response in guided-mode resonance filter design," Appl. Opt. **42**(16), 3225–3233 (2003).
11. C. F. R. Mateus, M. C. Y. Huang, L. Chen, C. J. Chang-Hasnain, and Y. Suzuki, "Broadband mirror (1.12-1.62 μm) using single-layer sub-wavelength grating," IEEE Photon. Technol. Lett. **16**(7), 1676–1678 (2004).
12. W. Suh, and S. Fan, "All-pass transmission or flattop reflection filters using a single photonic crystal slab," Appl. Phys. Lett. **84**(24), 4905 (2004).
13. S. Boutami, B. B. Bakir, H. Hattori, X. Letartre, J.-L. Leclercq, P. Rojo-Rome, M. Garrigues, C. Seassal, and P. Viktorovitch, "Broadband and compact 2-D photonic crystal reflectors with controllable polarization dependence," IEEE Photon. Technol. Lett. **18**(7), 835–837 (2006).

#128072 - $15.00 USD Received 6 May 2010; revised 9 Jun 2010; accepted 12 Jun 2010; published 16 Jun 2010

14. Y. Ding, and R. Magnusson, "Resonant leaky-mode spectral-band engineering and device applications," Opt. Express **12**(23), 5661–5674 (2004).
15. M. L. Wu, Y. C. Lee, C. L. Hsu, Y. C. Liu, and J. Y. Chang, "Experimental and Theoretical demonstration of resonant leaky-mode in grating waveguide structure with a flattened passband," Jpn. J. Appl. Phys. **46**(No. 8B), 5431–5434 (2007).
16. R. Magnusson, and M. Shokooh-Saremi, "Physical basis for wideband resonant reflectors," Opt. Express **16**(5), 3456–3462 (2008).
17. W. Zhou, Z. Ma, H. Yang, Z. Qiang, G. Qin, H. Pang, L. Chen, W. Yang, S. Chuwongin, and D. Zhao, "Flexible photonic-crystal Fano filters based on transferred semiconductor nanomembranes," J. Phys. D. **42**(23), 234007 (2009).
18. L. Coldren, and S. Corzine, *Diode lasers and photonic integrated circuits*, (Wiley New York, 1995).
19. J. H. Kim, L. Chrostowski, E. Bisaillon, and D. V. Plant, "DBR, Sub-wavelength grating, and Photonic crystal slab Fabry-Perot cavity design using phase analysis by FDTD," Opt. Express **15**(16), 10330–10339 (2007).
20. D. Babic, and S. Corzine, "Analytic expressions for the reflection delay, penetration depth, and absorptance of quarter-wave dielectric mirrors," IEEE J. Quantum Electron. **28**(2), 514–524 (1992).
21. C. Sauvan, J. Hugonin, and P. Lalanne, "Difference between penetration and damping lengths in photonic crystal mirrors," Appl. Phys. Lett. **95**(21), 211101 (2009).
22. M. Born, E. Wolf, and A. Bhatia, *Principles of optics: electromagnetic theory of propagation, interference and diffraction of light*: Cambridge Univ Pr, 1999.

1. Introduction

Ultra-compact dielectric broadband reflectors are essential elements in the design of laser cavities, light trapping microcavities, cavity QEDs, nonlinear optics, and quantum computing systems [1–4]. Traditionally, they can be realized by using the metal films or the stacked dielectric thin films (i.e., distributed Bragg reflectors, DBRs). Metal films can offer larger reflection bandwidth but are limited by the intrinsic absorption losses. Stacked dielectric thin films can achieve very low losses. But they typically require many individual layers with the stringent refractive index and thickness tolerances for each layer. Two dimensional photonic crystal slab (2D PCS) broadband reflectors can be realized for in-plane directions based on the photonic bandgap principle [5]. Recently more attention has been paid to the single layer patterned broadband reflectors for surface-normal incident direction operation, based on the guide mode resonance, or Fano resonance [6–8] principles, for single layer one-dimensional sub-wavelength grating (1D SWG) structures, or 2D PCS structures [8–17].

Under surface-normal incidence, DBR, 1D SWG, and 2D PCS reflectors can all exhibit similar reflection properties with extremely high reflection and broad reflection spectral band. However, reflection mechanisms are different. For 1D SWG and 2D PC mirrors, the incident wave couples to the in-plane guided-mode based on phase matching conditions. The wave then reradiates at one edge with a zero phase difference and at another edge with a π phase difference. Consequently, these constructive and destructive interferences result in high reflection and low transmission, respectively [16]. While for DBR, the high reflectivity arises from the multiple reflections with constructive interference among these reflected waves. Due to the large index difference, Bragg mirrors possess a broad reflection spectral band [18]. For 1D SWG and 2D PCS mirrors, the broad reflection spectral band most likely originates from the cooperating of the several adjacent guided mode resonances [16].

In addition to the reflector spectral amplitude properties, such as high reflectivity R and broad reflection band, it is equally important to understand the phase discontinuity and dispersion behavior (reflection phase shift, Φ_r), the field/energy penetration depths (L_p, L_e), and the field/cavity modal characteristics in cavities formed by these types of patterned single layer dielectric reflectors. However, most attentions so far have been paid to the spectral reflection amplitude properties. Very little work has been reported on phase/dispersion and mode/energy characteristics. In Ref [19], the authors reported excellent work on the phase discontinuity Φ_r and the energy penetration depth L_e, which were estimated from the mode spacing in the Fabry-Perot (FP) cavity. In this work, we investigate the phase discontinuity and the dispersion properties in 2D PCS Fano reflectors, for applications in multi-wavelength cavity design. We will also discuss the distinctively different behavior for phase and energy penetration depths. The phase penetration depth L_p is related to the reflection delay. A large

#128072 - $15.00 USD Received 6 May 2010; revised 9 Jun 2010; accepted 12 Jun 2010; published 16 Jun 2010

phase penetration depth will lead to longer photon lifetime and longer cavity resonance. The energy penetration depth L_e is related to the energy decay. A smaller energy penetration depth will lead to more modal confinement [18,20,21]. In addition, the different reflection mechanisms, guided mode resonance in PC mirrors and constructive interferences in DBRs, result in distinctively different field distribution profiles inside the cavity, which is another important factor to be considered in the laser cavity design. In what follows, we first introduce the cavity configurations of three types of surface-normal dielectric reflectors. Secondly, we investigate and compare the two penetration depths, L_p and L_e according to the calculated Φ_r and R values, based on the 3D finite difference time domain (FDTD) technique. We then compare the field distributions of the resonant modes in FP cavity formed by these three types of dielectric reflectors. Finally, a conclusion is given.

2. Dielectric mirrors configuration and corresponding FP cavities

Here, we consider three types of dielectric mirrors and their corresponding FP cavities, as shown in Fig. 1. They all consist of two kinds of materials, Si and SiO_2. Here Si and SiO_2 are assumed to be lossless and dispersion-free, with the refractive indexes are of 3.48 and 1.48, respectively, over the spectral range of interest around 1550 nm. In Fig. 1(a), the top and the bottom mirrors of the FP cavity (denoted as "Cavity I") are 1D Si SWG structures with the same lattice parameters, with the Si layer thickness h of 0.46μm, the grating period Λ of 0.7μm, and the air slit width w of 0.25Λ. The bottom SWG mirror is formed on a silicon-on-insulator (SOI) substrate, with the buffered oxide (BOX) layer thickness of 0.83μm. These two 1D SWG reflectors exhibit a high reflection over 1.1-2.06μm wavelength band for TM polarization only (H field is parallel to the air slit, y direction) [16].

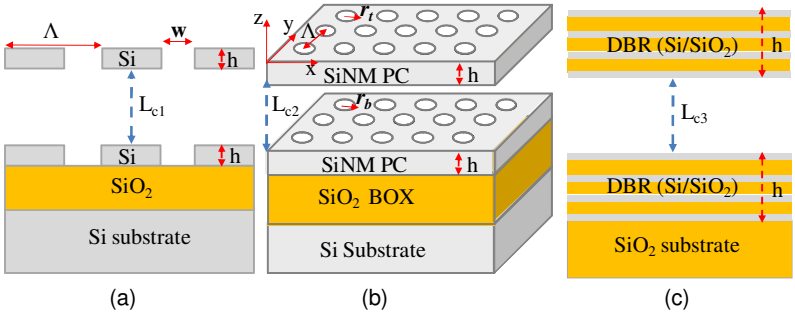

Fig. 1. Sketches of different dielectric reflectors and the corresponding Fabry-Perot cavities: (a) cross section (xz plane) of Cavity I consisting of top and bottom reflectors based on 1D single Si-layer sub-wavelength grating (SWG) with the same pattern parameters; (b) overview of Cavity II consisting of top and bottom mirrors based on 2D PCS patterns with a square air holes lattice; (c) cross section (xz plane) of Cavity III consisting of top and bottom mirrors based on 4-pairs of Si/SiO_2 (0.11/0.27μm) DBR stacked layers.

Shown in Fig. 1(b) is the second FP cavity ("Cavity II") formed with top and bottom 2D PCS Fano reflectors, where the Si slab layers with a thickness h = 0.34um are patterned with 2D square lattice air hole arrays. The PC lattice constant Λ is equal to 0.98μm. Again, the bottom reflector is processed on a SOI wafer, with the BOX layer thickness of 1μm. To enable the reflection bands of the top and bottom mirrors with large spectral overlap, their radius of air hole are set to r_t = 0.26Λ and r_b = 0.28Λ, respectively. The resulting overlapping reflection range of these two 2D PC mirrors is over 1.49-1.58μm wavelength band for both TE and TM polarizations (Broader and more flat band could be found through carefully optimizing the structure parameters). For comparison, we also consider the third FP cavity ("Cavity III"), based on two classical high index contract Si/SiO_2 DBRs, as shown in Fig. 1(c). The DBRs consist of 4-pairs of Si/SiO_2 stacked layers, where the thickness of Si and SiO_2 are chosen to be 0.11 and 0.27μm, respectively. Such a DBR with a very large index difference possesses a

#128072 - $15.00 USD Received 6 May 2010; revised 9 Jun 2010; accepted 12 Jun 2010; published 16 Jun 2010

wide reflection band over 1.22-2.07μm. Note all the parameters chosen here are optimized for broadband reflectors with peak reflection around 1550nm.

3. Phase penetration depth and energy penetration depth

In dielectric mirrors, the reflection is not an instantaneous process. It includes a reflection time delay (τ) and energy storage in the mirrors. The reflection delay increases the laser cavity round-trip time or the photon lifetime. The energy storage in mirrors decreases the modal volume and the confinement factor in small cavity in which the cavity round-trip time and the cavity volume have a comparable magnitude as the reflection delay and the mirror storage [20,21]. The reflection delay is directly related to the slope of the reflection phase shift Φ_r. The relation can be expressed as $\tau = \partial\Phi_r / \partial\omega$. The phase penetration depth, L_p, is defined as the half-distance that light propagates in the incident medium during this delay time,

$$L_p = \frac{1}{2} v_g \tau = \frac{v_g}{2} \frac{\partial \Phi_r}{\partial \omega}, \tag{1}$$

where v_g is the group velocity of the incident wave.

The energy storage is always associated to the parameter of energy penetration depth, L_e. It is the length that the field intensity decays to *1/e* of its maximum from the edge of cavity into the mirrors. However, this method is not suitable to calculate L_e of the PC mirrors we discuss here, because the guided modes are excited inside the mirrors. But L_e can be estimated from the mirror transmission or reflection based on the following equation,

$$T = 1 - R = \exp(-\frac{h}{L_e}), \tag{2}$$

where T is the transmission and h is the mirror thickness [18,21]. While, for DBRs, L_e can be obtained [18]:

$$L_e = \frac{m_{eff}}{2} (\frac{\lambda}{4n_1} + \frac{\lambda}{4n_2}), \tag{3}$$

where $m_{eff} = tanh(2mr)/(2r)$ is the effective period number seen by the incident light. $r = (n_1 - n_2)/(n_1 + n_2)$ and m is the actual period number in DBRs. n_1 and n_2 are the refractive index of two materials in DBR, respectively. In the following we will numerically investigate the phase and energy penetration depth according to the above definitions.

3.1 Reflection and the phase shift

First, we utilize FDTD simulation method to get R and Φ_r of these dielectric mirrors. A Gaussian temporal pulse excitation is used to simulate the reflectivity R. In order to calculate Φ_r, a continuous plane wave of a single wavelength (λ) is vertically incident on the dielectric mirrors and Φ_r is extracted from the stable reflected field. Here the calculated Φ_r is set in the range of [0, 2π]. In order to validate our numerical simulation method, we compare the simulated R and Φ_r of the top DBR based on FDTD with the theoretical calculated values according to the multiple thin film matrix theory [22]. The calculated results completely overlap with the theoretical ones.

Plotted in Fig. 2(a) are the simulated R and Φ_r values for both top and bottom DBRs. In the high reflection (R>0.95) spectral band, covering from 1.2 to 2.1μm, Φ_r slowly increases from 0.815π to 1.19π. Shown in Fig. 2(b) are the simulated R and Φ_r spectra of top and bottom 1D SWG reflectors. The high reflection TM (R>0.95) spectral band spans from 1.1 to 2.06μm. Although both DBR and 1D SWG reflector have similar broad high reflection spectra bands, their Φ_r changes are very different. Φ_r of 1D SWG reflector rapidly varies in the range of [0, 2π], much faster than those of DBRs. The calculated R and Φ_r spectra of for the top and

#128072 - $15.00 USD Received 6 May 2010; revised 9 Jun 2010; accepted 12 Jun 2010; published 16 Jun 2010

bottom 2D PCS reflectors are plotted in Fig. 2(c), where the overlapping high reflection spectra band covers from 1.49 to 1.58μm. Owing to the different air fill factors ($r_t = 0.26\Lambda < r_b = 0.28\Lambda$), high reflection spectral band for the bottom mirror is narrower than that of the top mirror. In this high reflection band range, the phase shift of top mirror Φ_{rt} varies in range of (0.91π, 1.17π), and the phase shift of bottom mirror Φ_{rb} changes in range of (0.7π, 1.14π). For all these three types of mirrors, Φ_r varies over the high reflection spectral band at drastically different change rates, which can be found by comparing the phase penetration depth L_p.

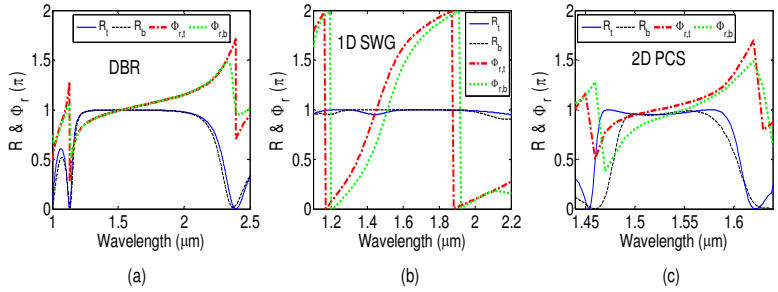

Fig. 2. Calculated reflection R (blue solid and black dash lines) and phase shift Φ_r (red dash-dot and green dot lines) spectra of top and bottom (a) DBR reflectors, (b) 1D SWG reflectors and (c) 2D PCS reflectors.

3.2 Phase penetration depth and energy penetration depth

The phase penetration depth L_p can then be calculated based on Eq. (1) and the simulated Φ_r shown in Fig. 2 The results are plotted in Fig. 3(a), for the bottom DBR, 1D SWG, and 2D PCS reflectors in the wavelength range of 1.5-1.6μm, denoted as $L_{p,\ DBR}$, $L_{p,\ 1DSWG}$, $L_{p,\ 2DPCS}$, respectively. It can be seen that $L_{p,\ 2DPCS}$ (~2.1μm) and $L_{p,\ 1DSWG}$ (~3.2μm) are one order larger than $L_{p,\ DBR}$ (~0.22μm). Additionally, while $L_{p,\ DBR}$ and $L_{p,\ 1DSWG}$ remains largely unchanged over the spectral range, $L_{p,\ 2DPCS}$ does change significantly over different spectral locations. This not only results in a much longer reflection delay time in PC mirrors, it also leads to different resonance cavity locations. Such a long phase delay may be due to the guided mode excitation, even if 2D PCS reflectors are very thin. To verify this point, we record the dynamic process of the reflected field with λ = 1.540μm at one monitor above the 2P PCS reflector and the DBR, as shown in Fig. 3(b). One can find, for the PCS reflector based on guided mode Fano resonance, the reflected field reaches stable condition only after a long 200fs period, while it only takes about 60fs for DBR to reach the stable condition. So, it is very clear these two different reflection mechanisms result in very different L_p values in PC reflectors and DBRs.

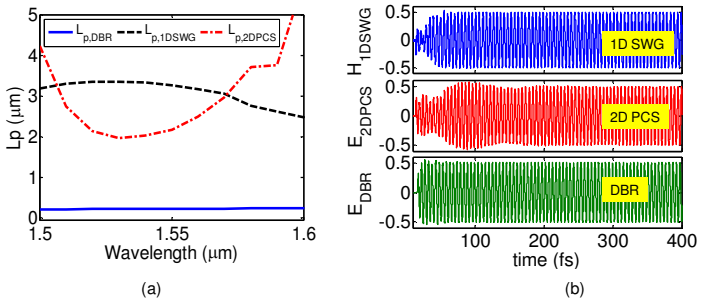

Fig. 3. (a) The phase penetration depths for three types of bottom reflectors; (b) Reflected field at λ = 1.540μm changes as function of time, for 1D SWG reflectors (top), 2D PCS reflectors (middle), and DBR reflectors (bottom).

#128072 - $15.00 USD Received 6 May 2010; revised 9 Jun 2010; accepted 12 Jun 2010; published 16 Jun 2010

The energy penetration depth L_e can be obtained based on $T = 1\text{-}R$, and Eqs. (2) and (3). The results are sown in Fig. 4 for the bottom DBR, 1D SWG, and 2D PCS reflectors, respectively. Different from the phase penetration characteristics discussed earlier, both $L_{e,\,2DPCS}$ (~100 nm) and $L_{e,\,1DSWG}$ (~60 nm) are much lower than $L_{e,\,DBR}$ (~220 nm). And all energy penetration depths have much less wavelength dependence, as compared to that of phase penetration depths. It is worth noting that much higher energy penetration depths are expected in DBRs with smaller index contrast (e.g. GaAs/AlGaAs, InGaAsP DBRs). Such a small energy penetration length in PCS mirrors can attribute from the tight mode confinement. This is also very favorable in achieving better modal confinement inside the cavity. For classical DBRs, the phase penetration depth is typically smaller or similar to the energy penetration depth, due to smaller index contract and larger energy penetration depth [18,22]. However, for 1D SWG and 2D PCS reflectors discussed here, L_p is much larger than L_e, consistent with in-plane 2D PCS reflectors, as reported in *Ref.* 18. This could be due to the large phase discontinuities originated from the modal interaction between in-plane guided modes and vertical radiation modes. On the other hand, the energy penetration depth can be very small and localized with the thin PCS layer.

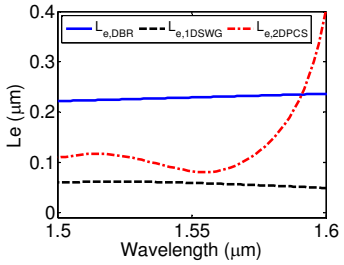

Fig. 4. The energy penetration depths for three types of bottom reflectors.

4. FP cavities and field distributions

Finally, for the resonant FP cavity modes, we can investigate the field distribution properties in these FP cavities shown in Fig. 1. To have resonance cavity modes with similar spectral locations, the cavity lengths are chosen as L_{c1} = 5.4μm, L_{c2} = 5.2 and 5.4μm, L_{c3} = 5.4μm in three different cavities. We chose the two resonant modes in each cavity: λ = 1.629μm and 1.510μm in Cavity I, λ = 1.504μm and 1.540μm in Cavity II, λ = 2.076μm and 1.540μm in Cavity III.

Figure 5(a) represents the field intensity of two resonant modes in DBR Cavity III, λ = 2.076μm and 1.540μm, where the dielectric index profile is also plotted with a black thin line. For a classical DBR cavity, the field intensity inside the cavity is always larger than that in mirrors, and the field gradually decays into the mirrors. However, it is not the case for Cavity I and II based on Fano or guided mode resonances. In Cavity I at L_{c1} = 5.4μm, for the two resonant modes (λ = 1.629μm and 1.510μm) shown in Fig. 5(b), the magnetic field intensity inside cavity is much smaller than that in mirrors. It is because the guide modes are excited into the mirrors. Outside the cavity, the field intensity decays rapidly, which is in consistent with the very small L_e obtained earlier. Figure 5(c) and Fig. 5(d) correspond to the case for Cavity II. It can be seen that the electric field intensity of the two resonant modes (λ = 1.504μm and 1.540μm) inside cavity is much larger than that in reflector slabs and the field outside cavity also decays very fast. Cases shown in Figs. 5(b)–5(d) can exist in both 1D SWG and 2D PCS based FP cavities. However, the ratio of the intensity inside the reflector slabs to the intensity inside the cavity (between two reflector slabs) is still larger than that of Cavity III, mostly due to nature of Fano or guide mode resonance excitation inside reflector slabs. Nevertheless, it is expected a very high modal confinement inside the cavity with high field intensity.

#128072 - $15.00 USD Received 6 May 2010; revised 9 Jun 2010; accepted 12 Jun 2010; published 16 Jun 2010

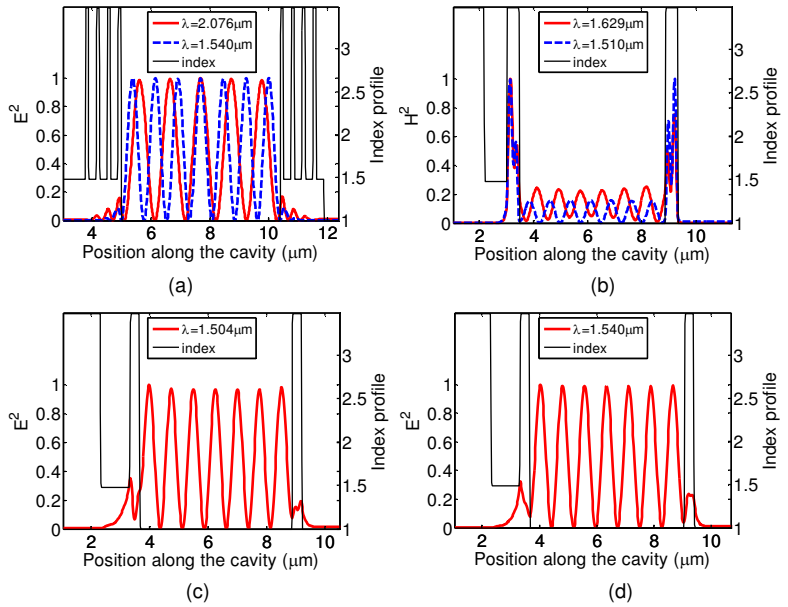

Fig. 5. Field intensity distributions of the resonant modes inside the cavities (a) Cavity III with L_{c3} = 5.4μm, (b) Cavity I with L_{c1} = 5.4μm, and (c) Cavity II with L_{c2} = 5.2μm, and (d) Cavity II with L_{c2} = 5.4μm.

5. Conclusion

In conclusion, we have numerically investigated phase and energy penetration depths, and field distributions of 1D SWG and 2D PCS reflectors based on Fano or guided mode resonances. Comparing to the DBR reflectors, these new types of single layer ultra-compact broadband reflectors can have more complicated larger phase delays and smaller energy penetration properties, which can be engineered via dispersion engineering for large spectral dependent phase delays, and ultra-small energy penetration depths. The work reported here is mostly based on one set of optimized design parameters for 1550nm band reflectors. Following similar procedures, other design parameters can be used for reflectors with different reflection requirements, as well as different phase delays, energy penetrations, and field distributions. All the results and conclusions can be very helpful for the design of resonant cavities for a wide range of photonic applications.

Acknowledgments

DZ appreciates the help from Dr. Zexuan Qiang. This work is supported in part by US Air Force Office of Scientific Research (AFOSR) MURI program under Grant FA9550-08-1-0337, by AFOSR under grant FA9550-09-C-0200, and in part by US Army Research Office (ARO) under Grant W911NF-09-1-0505.

#128072 - $15.00 USD Received 6 May 2010; revised 9 Jun 2010; accepted 12 Jun 2010; published 16 Jun 2010